IEEE Photonics Journal
An IEEE Photonics Society Publication

Open Access

Wavelength-Selective Optical Filters Based on Metal-Patch Cavities With Slot Waveguide Interfaces

Volume 6, Number 4, August 2014

Youngho Jung
Jong-Bum You
Kyungmook Kwon
Kyoungsik Yu

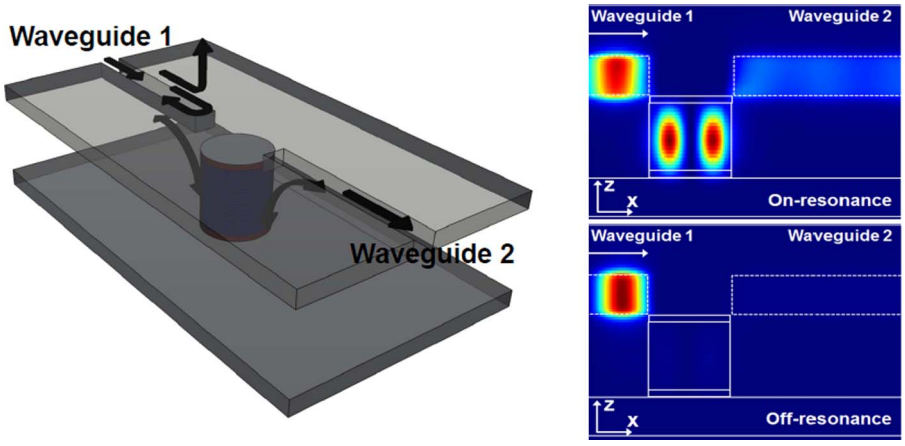

DOI: 10.1109/JPHOT.2014.2331253
1943-0655 © 2014 IEEE

IEEE photonics SOCIETY

IEEE

Wavelength-Selective Optical Filters Based on Metal-Patch Cavities With Slot Waveguide Interfaces

Youngho Jung, Jong-Bum You, Kyungmook Kwon, and Kyoungsik Yu

Department of Electrical Engineering, Korea Advanced Institute of Science and Technology (KAIST), Daejeon 305-701, Korea

DOI: 10.1109/JPHOT.2014.2331253

Manuscript received April 24, 2014; revised June 5, 2014; accepted June 6, 2014. Date of publication June 17, 2014; date of current version July 1, 2014. This work was supported in part by the National Research Foundation of Korea (NRF) under Grants 2008-0062256 and 2010-0002845 funded by the Korean Government (MEST) and in part by the Center for Integrated Smart Sensors funded by the Ministry of Science, ICT & Future Planning through the Global Frontier Project CISS-2012M3A6A6054191. Corresponding author: K. Yu (e-mail: ksyu@kaist.edu).

Abstract: We theoretically propose and investigate the resonant wavelength-selective optical filters based on the subwavelength metallo-dielectric nanopatch cavities and the metal slot waveguides. Using the temporal coupled-mode theory and three-dimensional finite-difference time-domain simulations, we analyze the optical coupling efficiencies and filtering characteristics, which are optimized by adjusting the waveguide-cavity distance to modify the decay rates from the cavity. The proposed optical filters can be extended to multiport channel-dropping filters while maintaining subwavelength-scale dimensions including the coupling regions.

Index Terms: Plasmonics, nanocavities, optical interconnects.

1. Introduction

Wavelength-selective optical filters are one of the essential components in optical signal processing and multi-channel communications to select/reject particular wavelength components from incoming wavelength-multiplexed signals [1]–[9]. Resonant optical filters based on dielectric materials, such as distributed feedback resonators [1], micro-ring/disk resonators [2], [3], and photonic crystal resonators [4], are attractive candidates to achieve precise wavelength selection in the photonic integrated circuit platform because of their well-known design rules and good optical performances with narrow pass/rejection bandwidths and low insertion losses. Their device sizes, however, occupy relatively large areas (typically on the order of several wavelengths in one dimension) mainly because of the diffraction limit. Recently, to implement ultra-compact optical filtering devices for highly dense photonic/plasmonic circuits, the wavelength-selective optical filters based on metal-based plasmonic cavities, such as plasmonic nano-ring/disk [5]–[7] and rectangular-shaped slots [8], [9], have been studied at the deep subwavelength scales. Although the filter dimensions can be significantly reduced, their performances, including the insertion losses and filter bandwidths, are usually limited by the metal absorption losses and inefficient waveguide coupling schemes.

In this paper, we propose a wavelength-selective optical filter based on a metallo-dielectric nanopatch cavity with metal slot waveguide interfaces. The patch-type cavities with

metal-semiconductor-metal layers have been intensively investigated theoretically and experimentally for light source applications due to their compact physical/modal volumes and modest quality factors [10]–[13]. The optical coupling scheme for such subwavelength-scale cavities, however, has been less studied because of various fundamental and practical issues, including modal mismatches between the dielectric waveguides and metallo-dielectric resonators as well as broad radiation patterns from the subwavelength-scale confinement [13]–[16]. As demonstrated in [13], for example, the nanopatch cavities can be coupled to the conventional dielectric rectangular waveguides with the coupling efficiency of $\sim$22% by placing the cylindrical semiconductor core at the off-axis position from the center of the metallic nanopatch structure to break the symmetry and thereby to modify the radiation field distribution. In this case, the optical coupling into the dielectric waveguides becomes less efficient because of mismatches in mode sizes and wavenumbers, and it is difficult to increase the number of input/output ports. To achieve higher integration densities and better optical filtering performances using the subwavelength-scale metallo-dielectric nanopatch cavities, a highly efficient and compact waveguide-cavity coupling scheme to overcome the broad radiation patterns is necessary. In this study, we introduce metal slot waveguides as efficient optical coupling interfaces for ultra-compact metallo-dielectric optical dropping filters and switches based on the metal-patch-type cavity with the metal-semiconductor-metal layers. High coupling efficiencies (up to 87%) between the metal-patch cavity and the slot waveguide result from efficient evanescent wave coupling and mode matching. The metal slot waveguides are well-known to support the strong subwavelength confinement of the propagating optical modes in wide frequency ranges with small bending radii and reasonable propagation lengths, and therefore have been considered as an important building block for optical/plasmonic signal interconnects and processing elements in high-density optical circuits [17]–[23].

To quantitatively analyze optical coupling and filtering characteristics based on the metal-patch cavities and slot waveguides, the temporal coupled-mode theory (CMT) was applied to account for radiation, absorption, and scattering losses. We also compared the temporal CMT with three-dimensional finite-difference time-domain (FDTD) simulations, and achieved excellent agreement. Enhanced coupling efficiencies and narrow-passband optical filtering could be obtained in telecommunication wavelengths. Furthermore, by taking advantages of the circularly symmetric field profile of the cavity mode (TE_{011}) and low crosstalk between the metal slot waveguides, the proposed cylindrical metal-patch cavity filter can support multiple input/output ports within a small footprint, which is difficult with purely dielectric counterparts due to their dimensions and non-negligible interferences/crosstalks.

2. Structures and Mode Properties

Fig. 1 schematically shows the proposed resonant wavelength-selective filter configuration with the metallo-dielectric nanopatch cavity and the metal slot waveguide coupling interfaces. The extended metal-patch cavity consists of a cylindrical dielectric core layer with a high refractive index non-absorbing semiconductor material (e.g., silicon or compound semiconductor such as indium phosphide for near infrared wavelengths) sandwiched between two metal (Ag in our simulations) layers much larger than the cylinder area to minimize the radiation losses as described in [13]. The resonant frequencies of the cavity modes are dependent mainly on the dielectric cylindrical core geometries. In our computer simulations based on the three-dimensional FDTD method, the height (h) and radius (r) of the cylindrical semiconductor material are $h = 300$ nm and $r \sim 250$ nm, respectively, at which the magnetic dipole-like TE_{011} mode is supported at $\sim$1510 nm and the electrical dipole-like TM_{111} exists at near 1660 nm. In the following analysis, we focus our attention on the TE_{011} mode because its overall quality factor (Q) is larger than that of TM_{111} [11], which results in better coupling efficiency and narrower bandwidth filtering. We assume that the thickness of the top and bottom metal layers $(t_{metal} = 150$ nm$)$ is thicker than the skin depth at near-infrared wavelengths to suppress unnecessary out-of-plane radiation. To reduce dissipative absorption losses in the metal layers, low-index dielectric (SiO_2)

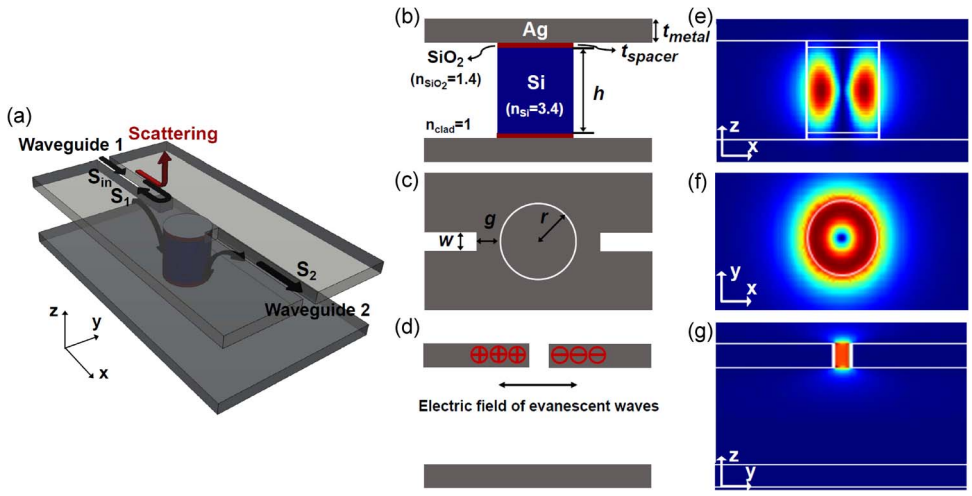

Fig. 1. Device structures and mode profiles. (a) Perspective schematic as well as (b) front (x-z plane), (c) top (x-y plane), and (d) side (y-z plane) views of the proposed metallo-dielectric wavelength-selective optical filter based on the metal-patch cavity and the metal slot waveguide interfaces. (e, f) The electric field magnitude profiles ($|E_\phi|$) of the cavity mode (TE_{011}). (g) The electric field magnitude profile ($|E_y|$) for the slot waveguide mode.

spacer layers with the thickness of $t_{spacer} = 20$ nm are inserted between the cylindrical core material and the metal layers [13]. For practical implementation, the cladding layer outside the cylindrical core can be planarized by a low-index dielectric resist such as described in [24]. However, to bring out the essential physics and make our analysis simple, the cladding layer is assumed to be air. We adopt the known experimental values for the permittivity of silver at room temperature near 1500 nm [25], and use the refractive index of 1.4 and 3.4 for the dielectric spacer layer and the core semiconductor materials, respectively, for the whole wavelength range of interest in our simulation. The perfectly matched layer (PML) boundary conditions are employed to absorb all outgoing radiation with zero reflection. A nonuniform computational mesh is used and the minimum mesh grid size in the structure is set to be 5 nm. We found the unloaded quality factor of $\sim$950 for the TE_{011} mode of the metal-patch cavity without external waveguiding structures, which has enough photon lifetimes for optical wavelength-selective filtering. The cavity quality factor can be further improved by controlling the spacer thicknesses and its refractive index.

The optical coupling efficiency between the cavity and access waveguides heavily relies on the electromagnetic field distributions of the resonant and guided modes [13]–[16]. The electric field profile of the TE_{011} mode circulates around the dielectric cylinder with a donut shape as described in Fig. 1(e) and (f). The direction of the evanescent electric field from the cavity is therefore parallel to the propagating mode of the slot waveguide (in-plane electric field), resulting efficient mode matching. The evanescent electric field induces charge accumulation at the opposite edges of the metal slot waveguides [Fig. 1(d)], and creates a horizontal electric field (E_y) within the slot region [26]. This slot waveguide mode provides reasonable propagation losses and strong light confinement beyond the classical diffraction limit for high-density photonic integrated circuits [17], [18]. In our work, the metal slot width is set to be $w = 50$ nm considering the balance between the propagation loss and fabrication tolerances for, for example, a focused ion beam milling (FIB) method on the top metal layer [27]. On the top view, the cylindrical core and the slot waveguides are separated by the gap (g) as shown in Fig. 1(c). According to our simulation results, the lowest order mode for the metal slot waveguide with $w = 50$ nm is the slot surface plasmon polaritons mode with an effective index of $\sim$1.32 and propagation loss of ~ 0.14 dB/μm around the wavelength range of interest at room temperature. The cross-sectional slot waveguide mode profile is plotted in Fig. 1(g) and indicates strong field confinement in the slot region. Even though the propagation loss of the metal slot waveguides is much

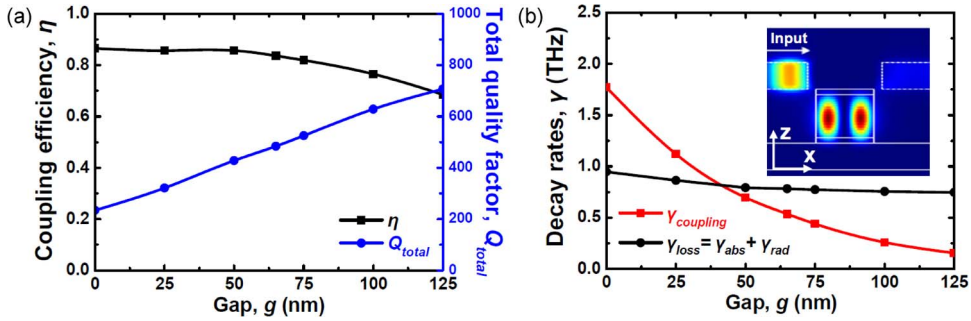

Fig. 2. (a) Coupling efficiency η and total quality factor Q_{total} of the metal-patch cavity as a function of the gap g between the cavity and the waveguides. (b) Decay rates of the coupling into waveguides ($\gamma_{coupling}$), and sum of absorption and radiation decay ($\gamma_{abs} + \gamma_{rad}$). The inset shows the field intensity distribution ($|E|^2$) along the cross-sectional x-z plane when the total cavity energy is maximized. A transverse-magnetic polarized incident wave was launched at the metal slot waveguide. The parameters of the coupling structure were set as $r = 240$ nm, $h = 300$ nm, and $w = 50$ nm.

higher than that of dielectric waveguides, its propagation length ($\sim$30 μm) is reasonable considering the small device footprints, and it is feasible to form a network of cascaded optical cavities within the propagation range for more advanced filtering and switching applications.

3. Optical Coupling Scheme

The light coupling of the TE_{011} cavity mode to/from the metal slot waveguides can be modeled by the temporal CMT. We assume the one-input and two-output case with two straight metal slot waveguides [waveguide 1 and 2 in Fig. 1(a)] where the resonant mode is excited by an incident forward-propagating wave (S_{in}) from the waveguide 1, and the excited cavity mode energy symmetrically couples out to two waveguides (S_1, S_2) away from the metal-patch cavity. The dynamic equation for the field amplitude, a of the cavity mode is given by [28] and [29]

$$\begin{aligned} \frac{da}{dt} &= (j\omega_0 - \gamma_{abs} - \gamma_{rad} - \gamma_{coupling})\, a + \sqrt{\gamma_{coupling}} S_{in} \\ S_1 &= e^{j\beta x}(rS_{in} + \sqrt{\gamma_{coupling}}\, a) \\ S_2 &= e^{j\beta x}(tS_{in} + \sqrt{\gamma_{coupling}}\, a) \end{aligned} \tag{1}$$

where ω_0 is the resonant angular frequency, and γ_{abs}, γ_{rad}, and $\gamma_{coupling}$ stand for the decay rates from the metal absorption, radiation into free space, and coupling into the waveguides, respectively. The quality factors can be derived from the decay rates, $Q = \omega/2\gamma$. For example, the absorption quality factor is given by $Q_{abs} = \omega/2\gamma_{abs}$. β is the complex propagation constant of the metal slot waveguide mode. r indicates the reflection toward the waveguide 1, and t is the direct transmission from the incidence to the opposite waveguide 2. S_{in}, S_1, and S_2 are the field amplitudes of the incoming and two outgoing waves from the cavity, respectively. To account for the waveguide loss, S_1 and S_2 are obtained at the distance x from the end facet of waveguide 1 and 2, respectively.

We used the three-dimensional FDTD method to analyze the coupling efficiencies and wavelength-dependent transmission characteristics through the metal-patch cavity. The simulation geometry is the same with Fig. 1. The waveguide-cavity coupling efficiency is defined as $\eta = \gamma_{coupling}/(\gamma_{rad} + \gamma_{coupling})$, which is the ratio of the waveguide-coupled optical power to the total radiated power from the cavity. Fig. 2(a) plots the coupling efficiency η and the total loaded quality factor with two metal slot waveguides as a function of the waveguide-cavity gap, g. The coupling efficiency monotonically decreases with the waveguide-cavity gap size due to the extra decay through the evanescent wave away from the cavity core. The coupling efficiency is

enhanced up to ~87% as the gap size is reduced, while the loaded quality factor decreases monotonically because of the electromagnetic energy leakage through the waveguides.

It is also possible to investigate the degree of waveguide-cavity coupling by calculating the steady-state cavity energy from the temporal CMT. The total cavity energy $|a|^2$ at the resonant frequency from (1) is given by

$$|a|^2 = \frac{\gamma_{coupling}}{(\gamma_{abs} + \gamma_{rad} + \gamma_{coupling})^2} |S_{in}|^2. \tag{2}$$

The amount of the total cavity energy is proportional to $\gamma_{coupling}/(\gamma_{abs} + \gamma_{rad} + \gamma_{coupling})^2$, which is maximized when the coupling rate into the waveguides $(\gamma_{coupling})$ matches with the sum of the absorption and radiation rates $(\gamma_{abs} + \gamma_{rad} = \gamma_{loss})$. $\gamma_{coupling}$ and γ_{loss} are plotted in Fig. 2(b) as a function of the waveguide-cavity gap, g. We note that γ_{loss} is almost constant regardless of the gap distance, g, because most optical power dissipation occurs within the cylindrical core region and not at the coupling section, whereas $\gamma_{coupling}$ is strongly dependent on the gap due to the evanescent wave coupling process. $\gamma_{coupling}$ becomes almost equal to γ_{loss} near $g \sim 40$ nm. The maximum cavity energy is calculated to be ~0.3 fJ when the input power is 1 mW. The inset of Fig. 2(b) shows the field intensity profile $(|E|^2)$ in the cross-sectional x-z plane at the middle of the metal slot waveguides to show the amount of energy coupled into the cylindrical cavity core from the incident wave.

4. Wavelength-Selective Optical Filters

4.1. The Performance of Wavelength-Selective Dropping Filters

The characteristics of the optical dropping filters are demonstrated by analyzing the coupling of the resonant modes to/from the input and output waveguides in the time domain. According to the CMT results, the performance of the proposed filter is limited by the intrinsic losses. To achieve critical coupling where the back reflection from the filter is completely suppressed, two slot waveguides can be asymmetrically positioned with non-equal spacing from the resonator. However, when the extra out-of-plane coupling losses (i.e., scattering losses, s) resulting from the end of the metal slot waveguides as shown in Fig. 1(a) are considered, the critical coupling condition should be modified and we can get almost zero reflectance by optimizing the coupling structure. The reflection and transmission coefficients as a function of the input angular frequency ω can be obtained from (1), which represents the fundamental equations of the optical cavities coupled to the output waveguides. The reflectance in the steady state is given by

$$R = \left|\frac{S_1}{S_{in}}\right|^2 = e^{-2\mathrm{Im}\{\beta\}d} \left| r + \frac{\gamma_{coupling}}{j(\omega - \omega_0) + \gamma_{abs} + \gamma_{rad} + \gamma_{coupling}} \right|^2 \tag{3}$$

where d is the round-trip distance from the input to the output observation point ($d = 1$ μm in our simulations) and r is a real number with $r^2 + t^2 + s^2 = 1$. The transmittance, $T = |S_2/S_{in}|^2$, can be obtained similarly with the reflectance. At resonance $(\omega = \omega_0)$, the reflectance dip reaches zero when the condition $(\gamma_{abs} + \gamma_{rad})/\gamma_{coupling} = -(1 + r)/r$ is satisfied. The transmission peak is only related to the waveguide-cavity coupling, $\gamma_{coupling}$, because the direct transmission of the incident wave to the opposite waveguide 2 is found to be very low $(t \sim 0)$ in our situation.

Three-dimensional FDTD simulations were carried out to find the transmission and reflection spectra as well as the decay rates from the proposed optical filtering structure. The FDTD simulation and the corresponding CMT results of the wavelength-dependent reflectance and transmittance are shown in Fig. 3. The theoretical responses of (3) fit very well with the FDTD

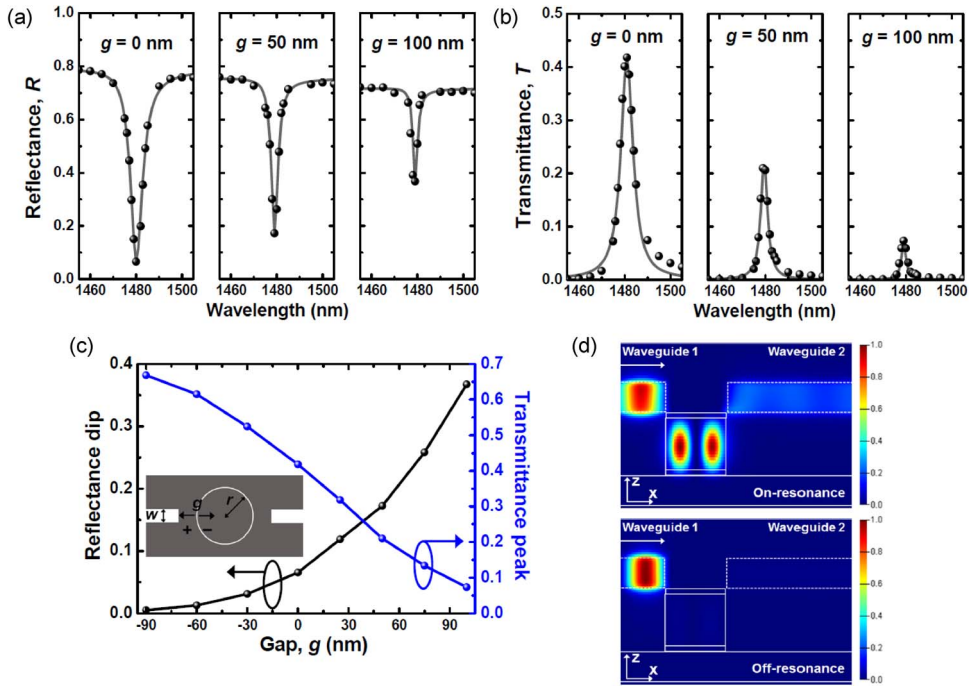

Fig. 3. (a) Reflectance (R) and (b) transmittance (T) spectra of the wavelength-selective dropping filter with different waveguide-cavity gap sizes. The circles and solid lines indicate the results of FDTD simulations and CMT, respectively. (c) Reflectance dip and transmittance peak as a function of the gap. (d) Field intensity distributions $(|E|^2)$ for resonant wavelength (1478 nm) and off-resonant wavelength (1500 nm). The parameters of the filter structure were set as $r = 240$ nm, $h = 300$ nm, and $w = 50$ nm.

simulation results, and show that the reflection (transmission) spectra exhibit Lorentzian-shaped profiles with stop (pass) band near the resonant wavelength of the TE_{011} cavity mode. As the waveguide-cavity gap g increases, the reflection dip (reflectance minimum) increases and the transmission peak decreases because of the low coupling rates $(\gamma_{coupling})$. The reflectance dip with the full width at half maximum (FWHM) of ~2.5 nm reaches ~37% while the transmittance and scattering losses are estimated to be ~7% and ~28%, respectively, for $g = 100$ nm. In such an under-coupling regime, significant portion of the remained power (~28%) is absorbed by the metal layers. If the end of the metal slot waveguide is not abruptly finished as in this simulation, but modified with a more careful design, the out-of-plane scattering can be significantly reduced. The detailed end facet design to maximize the energy transfer is beyond the scope of this paper. Nevertheless, we can approach the mentioned condition for better optical filtering (lower resonant reflection dip and higher transmission peak) by reducing the gap g to increase the coupling rates $(\gamma_{coupling})$, as shown in Fig. 2(b), although the operating bandwidth monotonically broadens up to ~7 nm. As a result, when the gap is $g = 0$ nm, the reflectance dip reaches close to zero [the left panel of Fig. 3(a)] and the transmission peak increases to ~42% [the left panel of Fig. 3(b)]. If the metal slot waveguides are positioned even closer to the cavity (i.e., on top of the cylinder core), the waveguide-cavity coupling rates $(\gamma_{coupling})$ can be increased much more and we can achieve almost zero reflection dip and higher transmission peak as shown in Fig. 3(c).

Fig. 3(d) shows the distributions of electric field intensity $(|E|^2)$ at the incident wavelengths of 1478 nm and 1500 nm, respectively. The cavity mode is strongly excited and couples into the output waveguides at the resonant wavelength (1478 nm). However, at off-resonance (1500 nm), there is almost no energy in the cavity and the incident wave does not propagate toward the output waveguide 2 as the most input energy is reflected back to the waveguide 1.

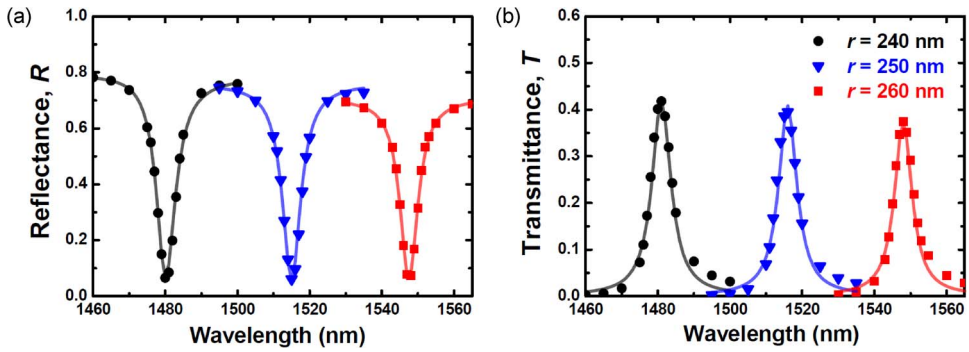

Fig. 4. Control of the center wavelength. (a) Reflectance and (b) transmittance spectra of the wavelength-selective optical filters with different cylinder radii (240 nm, 250 nm, and 260 nm). The symbols (circle, triangle, rectangular) and solid lines indicate the results of FDTD simulations and CMT, respectively. The parameters of the filter structure were set as $g = 0$ nm and $w = 50$ nm.

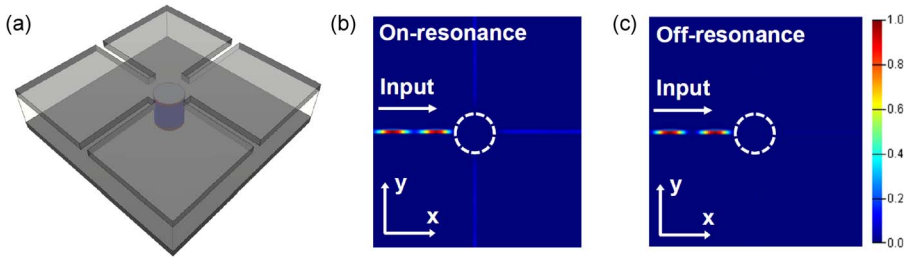

Fig. 5. (a) Schematic diagram of the wavelength-selective dropping filters with multiple ports. The electric field intensity profiles ($|E|^2$) in the cross-sectional x-y plane at (b) on- (1515 nm) and (c) off-resonant wavelength (1560 nm) are also shown.

We also study the effect of the cavity cylinder core radius to control the center wavelength of the optical passband. Fig. 4 shows the reflection and transmission spectra for different core radii (240 nm, 250 nm, and 260 nm), revealing that the center wavelengths shift toward longer wavelengths with the cylinder core radius because the resonant wavelength of the cavity mode increases almost linearly with the core radius [11] and [12]. Although not shown here, it is also possible to tune the resonant wavelength by changing the refractive index of the dielectric cylindrical core material with electro- or thermo-optic effects. Due to the compact filter dimensions, we expect to achieve smaller power consumption and/or faster tuning speed when compared to the conventional dielectric material-based optical filters.

4.2. Wavelength-Selective Dropping Filters With Multiple Ports

As shown in Fig. 5(a), the proposed filter structure can be extended to multiple input/output waveguides without much increasing the overall device footprints for the coupling regions (0.037 cubic wavelengths). In the conventional dielectric wavelength add-drop filters, for example, based on micro-ring resonators [2] and [3], it is difficult to avoid interferences and crosstalks between the output waveguides within subwavelength-scale dimensions. Especially when the resonator dimension approaches the diffraction limit, the waveguide width becomes comparable to the resonator itself and it is hard to place multiple access waveguides around the resonator. However, the metal slot waveguides allow more compact fan-in and fan-out interfaces mainly due to the strong localization of light with smaller bending radii. Moreover, from the rotationally symmetric profile of the TE_{011} cavity mode, when the output slot waveguides are symmetrically placed in the radial direction from the cylindrical core as shown in Fig. 5(a), our proposed structure can function as multi-port channel-dropping filters at the resonant

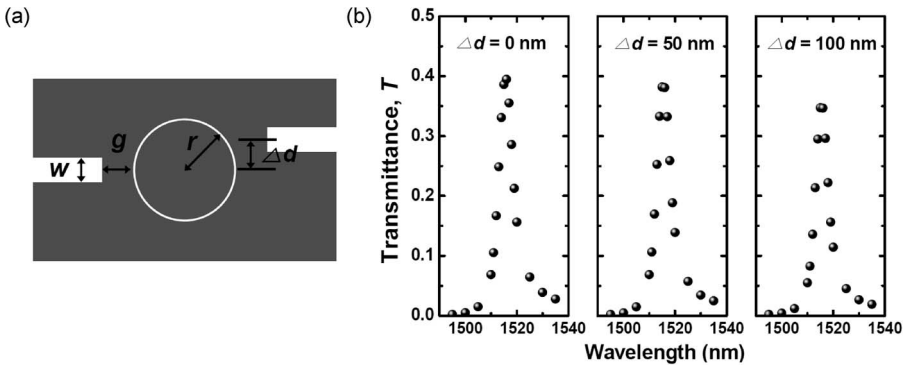

Fig. 6. Fabrication tolerance. (a) Schematic structure (top view) of the wavelength-selective dropping filter with the output metal slot waveguide offset Δd. (b) Transmittance spectra for different lateral offsets ($\Delta d = 0, 50,$ and 100 nm). The parameters of the filter structure were set as $r = 250$ nm, $g = 0$ nm, and $w = 50$ nm.

wavelengths. As an example, the electric field intensity profiles of a four-port optical filter at the resonant and off-resonant conditions are plotted in Fig. 5(b) and (c). They show that the incident wave efficiently couples toward the output ports through the center cavity at the resonant wavelength and the input optical power is equally distributed into each output ports due to the symmetry. The number of output ports can be easily increased by adding more metal slot waveguides around the cavity structure. Since it can function as a wavelength-selective broadcasting element for multiple output waveguides by distributing a target wavelength component from the incoming wavelength-multiplexed signals, the proposed device can be a building block of wavelength-selective switches based on the broadcast-and-select optical network architecture when multiple devices are cascaded. To separate the backward-propagating off-resonant wavelength components from the input waveguide, an additional optical circulator at the input waveguide is required. Recently, there are several experimental efforts to integrate optical circulators and isolators on the integrated photonics platforms [30]–[32], and such techniques can provide the output port for the reflected wavelength components.

4.3. Fabrication Tolerance

The proposed device can be fabricated as follows. A 20 nm-thick SiO_2 and 300 nm-thick a-Si are first deposited on a silicon substrate. The a-Si cylindrical core is defined by electron beam lithography and reactive ion etching. After patterning, the cladding layer is deposited and subsequently planarized for the deposition of the top metal patch layer. The SiO_2 layer can be deposited by plasma-enhanced chemical vapor deposition (PECVD) or atomic layer deposition (ALD), and followed by electron beam evaporation of the metal layer. The sample is then flipped and bonded to a supporting substrate, and the silicon substrate is removed. The metal layer is deposited again, and the slot waveguides are defined by FIB. To enhance the refractive index contrast, the cladding layer can be removed by a wet etch process [22]. The detailed fabrication process of the proposed filter structure is in progress and will be reported.

To assess the fabrication tolerance, we analyze the effect of the lateral offset Δd between the center of the dielectric cylindrical core and the metal slot waveguide. Fig. 6 shows the top view of the proposed optical dropping filter with the lateral offset in the output waveguide and the corresponding transmission spectra. The center wavelengths and bandwidths of the filter are almost not affected by the lateral waveguide offset Δd. The transmittance peak values are slowly reduced with Δd, but we can maintain strong coupling even when the output waveguide is not perfectly aligned because of the symmetric nature of the TE_{011} cavity mode. The axial misalignment corresponds to the variation of the gap distance between the cylindrical resonator and the end facet of the metal slot waveguide. Since the effect of such gap distance variation has been studied in previous Sections 3 and 4.1 (Figs. 2 and 3), we omit the detailed analysis

for the axial misalignment here. When misalignments in both directions are simultaneously present, the peak transmittance reduction would depend on the overall distance between the resonator and waveguide end due to the evanescent coupling process.

5. Conclusion

We have theoretically demonstrated an optical filtering scheme based on the metallo-dielectric cavity with the compact waveguide-cavity coupling interfaces using the temporal CMT and FDTD simulations. The metal slot waveguides can efficiently transfer the electromagnetic energy from/to the metal-patch cavities without much affecting the important optical properties of the resonant mode. The similarities of the electric field distribution between the TE_{011} cavity mode and the guided mode in the metal slot waveguides results high evanescent coupling efficiencies. The characteristics of wavelength-selective filtering are optimized by adjusting the decay rates, and the center wavelength of the optical passband can be easily modified by controlling the cylindrical dielectric core dimensions. By taking advantages of the symmetric resonant mode profiles and the strong light localization of the metal slot guided mode, it is feasible to implement the multi-port optical filters within subwavelength scales. We believe that the optical coupling interfaces and filtering scheme discussed in this study represent important building blocks that can enable efficient routing of optical signals between highly integrated subwavelength-scale optical components.

References

[1] H. A. Haus and Y. Lai, "Narrow-band optical channel-dropping filter," *J. Lightw. Technol.*, vol. 10, no. 1, pp. 57–62, Jan. 1992.
[2] B. E. Little, S. T. Chu, H. A. Haus, J. Foresi, and J.-P. Laine, "Microring resonator channel dropping filters," *J. Lightw. Technol.*, vol. 15, no. 6, pp. 998–1005, Jun. 1997.
[3] A. Morand *et al.*, "Ultra-compact microdisk resonator filters on SOI substrate," *Opt. Exp.*, vol. 14, no. 26, pp. 12 814–12 821, Dec. 2006.
[4] P. B. Deotare, M. W. McCutcheon, I. W. Frank, M. Khan, and M. Lončar, "High quality factor photonic crystal nanobeam cavities," *Appl. Phys. Lett.*, vol. 94, no. 12, pp. 121106-1–121106-3, Mar. 2009.
[5] Z. Han, V. Van, W. N. Herman, and P. T. Ho, "Aperture-coupled MIM plasmonic ring resonators with sub-diffraction modal volumes," *Opt. Exp.*, vol. 17, no. 15, pp. 12 678–12 684, Jul. 2009.
[6] H. Lu, X. Liu, D. Mao, L. Wang, and Y. Gong, "Tunable band-pass plasmonic waveguide filters with nanodisk resonators," *Opt. Exp.*, vol. 18, no. 17, pp. 17 922–17 927, Aug. 2010.
[7] T. B. Wang, X. W. Wen, C. P. Yin, and H. Z. Wang, "The transmission characteristics of surface plasmon polaritons in ring resonator," *Opt. Exp.*, vol. 17, no. 26, pp. 24 096–24 101, Dec. 2009.
[8] A. Noual, A. Akjouj, Y. Pennec, J. Gillet, and B. Djafari-Rouhani, "Modeling of two-dimensional nanoscale Y-bent plasmonic waveguides with cavities for demultiplexing of the telecommunication wavelengths," *New J. Phys.*, vol. 11, no. 10, p. 103 020, Oct. 2009.
[9] B. Yun, G. Hu, and Y. Cui, "Theoretical analysis of a nanoscale plasmonic filter based on a rectangular metal–insulator–metal waveguide," *J. Phys. D, Appl. Phys.*, vol. 43, no. 38, p. 385 102, Sep. 2010.
[10] C. Manolatou and F. Rana, "Subwavelength nanopatch cavities for semiconductor plasmon lasers," *IEEE J. Quantum Electron.*, vol. 44, no. 5, pp. 435–447, May 2008.
[11] K. Yu, A. M. Lakhani, and M. C. Wu, "Subwavelength metal-optic semiconductor nanopatch lasers," *Opt. Exp.*, vol. 18, no. 9, pp. 8790–8799, Apr. 2010.
[12] A. M. Lakhani, K. Yu, and M. C. Wu, "Lasing in subwavelength semiconductor nanopatches," *Semicond. Sci. Technol.*, vol. 26, no. 1, p. 014013, Nov. 2011.
[13] Q. Ding, A. Mizrahi, Y. Fainman, and V. Lomakin, "Dielectric shielded nanoscale patch laser resonators," *Opt. Lett.*, vol. 36, no. 10, pp. 1812–1814, May 2011.
[14] M.-K. Kim, A. M. Lakhani, and M. C. Wu, "Efficient waveguide-coupling of metal-clad nanolaser cavities," *Opt. Exp.*, vol. 19, no. 23, pp. 23 504–23 512, Nov. 2011.
[15] M.-K. Kim *et al.*, "Engineering of metal-clad optical nanocavity to optimize coupling with integrated waveguides," *Opt. Exp.*, vol. 21, no. 22, pp. 25 796–25 804, Nov. 2013.
[16] C.-W. Lee, G. Singh, and Q. Wang, "Light extraction–A practical consideration for a plasmonic nano-ring laser," *Nanoscale*, vol. 5, no. 22, pp. 10 835–10 838, Oct. 2013.
[17] G. Veronis and S. Fan, "Guided subwavelength plasmonic mode supported by a slot in a thin metal film," *Opt. Lett.*, vol. 30, no. 24, pp. 3359–3361, Dec. 2005.
[18] W. Cai, W. Shin, S. Fan, and M. L. Brongersma, "Elements for plasmonic nanocircuits with three-dimensional slot waveguides," *Adv. Mater.*, vol. 22, no. 45, pp. 5120–5124, Sep. 2010.
[19] Y. Bian and Q. Gong, "Low-loss hybrid plasmonic modes guided by metal-coated dielectric wedges for subwavelength light confinement," *Appl. Opt.*, vol. 52, no. 23, pp. 5733–5741, Jul. 2013.

[20] D. Pan, H. Wei, and H. Xu, "Optical interferometric logic gates based on metal slot waveguide network realizing whole fundamental logic operations," *Opt. Exp.*, vol. 21, no. 8, pp. 9556–9562, Apr. 2013.
[21] A. Kriesch *et al.*, "Functional plasmonic nano-circuits with low insertion and propagation losses," *Nano Lett.*, vol. 13, no. 9, pp. 4539–4545, Aug. 2013.
[22] K. C. Y. Huang *et al.*, "Electrically driven subwavelength optical nanocircuits," *Nat. Photon.*, vol. 8, no. 3, pp. 244–249, Feb. 2014.
[23] Y. Bian and Q. Gong, "Optical performance of one-dimensional hybrid metal–insulator–metal structures at telecom wavelength," *Opt. Commun.*, vol. 308, no. pp. 30–35, Nov. 2013.
[24] M. Zegaoui, J. Harari, N. Choueib, V. Magnin, and D. Decoster, "Quick planarisation based on Hydrogen Silses-Quioxane (HSQ) for deep etched InP based structures," *Electron. Lett.*, vol. 43, no. 22, pp. 1234–1236, Oct. 2007.
[25] P. B. Johnson and R. W. Christy, "Optical constants of the noble metals," *Phys. Rev. B, Condens. Matter*, vol. 6, no. 12, pp. 4370–4379, Dec. 1972.
[26] M. A. Seo *et al.*, "Terahertz field enhancement by a metallic nano slit operating beyond the skin-depth limit," *Nat. Photon.*, vol. 3, no. 3, pp. 152–156, Feb. 2009.
[27] D. F. P. Pile *et al.*, "Two-dimensionally localized modes of a nanoscale gap plasmon waveguide," *Appl. Phys. Lett.*, vol. 87, no. 26, pp. 261 114-1–261 114-3, Dec. 2005.
[28] H. A. Haus, *Waves and Fields in Optoelectronics*: Prentice-Hall, Englewood Cliffs, NJ, USA, 1984.
[29] W. Suh, Z. Wang, and S. Fan, "Temporal coupled-mode theory and the presence of non-orthogonal modes in loss-less multimode cavities," *IEEE J. Quantum Electron.*, vol. 40, no. 10, pp. 1511–1518, Oct. 2004.
[30] L. Bi *et al.*, "On-chip optical isolation in monolithically integrated non-reciprocal optical resonators," *Nat. Photon.*, vol. 5, no. 12, pp. 758–762, Nov. 2011.
[31] L. Fan *et al.*, "An all-silicon passive optical diode," *Science*, vol. 335, no. 6067, pp. 447–450, Jan. 2012.
[32] H. Lira, Z. Yu, S. Fan, and M. Lipson, "Electrically driven nonreciprocity induced by interband photonic transition on a silicon chip," *Phys. Rev. Lett.*, vol. 109, no. 3, pp. 033901-1–033901-5, Jul. 2012.